



Conformal reconfigurable holographic metasurface for multifunctional radiation and scattering modulation

XINYU ZHANG,¹  YUCHEN GAO,^{1,*}  WEI HU,¹  QI LUO,²
TAO HONG,¹ KAI-DA XU,³  AND WEN JIANG¹

¹School of Electronic Engineering, Xidian University, Xi'an 710071, China

²School of Physics, Engineering and Computer Science, University of Hertfordshire, Hatfield, AL10 9AB, United Kingdom

³School of Information and Communications Engineering, Xi'an Jiaotong University, Xi'an 710049, China
*gaoyuchen@xidian.edu.cn

Abstract: A reconfigurable holographic metasurface (HM) with multifunctional modulation of radiation and scattering for conformal applications is designed in this paper. Based on optical holography theory, a holographic conformal modulation mechanism is proposed, and the conformal surface impedance distribution of HM is derived. To illustrate this mechanism, the designed conformal reconfigurable HM is used to demonstrate a series of radiation and scattering modulation functions, with its reconfigurable property enabling dynamic beam control. In radiation mode, beam scanning with wide angle from -50° to 50° is achieved. In scattering mode, specific responses are generated under different incident angles, including beam steering under oblique incidence within $\pm 60^\circ$, multi-beam splitting within $\pm 60^\circ$ under normal incidence, and diffuse reflection. Low radar cross section (RCS) is exhibited over a wide frequency band from 7.2 to 25 GHz. The designed conformal reconfigurable HM shows high adaptability to cylindrical platforms, insensitivity to oblique incidence, and stability in beam deflection angles, which provides an innovative technical approach for information transmission and stealth in conformal devices.

© 2025 Optica Publishing Group under the terms of the [Optica Open Access Publishing Agreement](#)

1. Introduction

In the field of electromagnetic wave manipulation, metasurfaces are widely used in beam forming systems due to their extraordinary electromagnetic wave modulation capabilities [1–5]. The need for conformal metasurfaces is becoming increasingly apparent in non-planar structures such as aircraft, vessels, and unmanned aerial vehicles (UAVs), where effective control of electromagnetic waves is required to enhance stealth in communication and radar systems [6,7]. The development of reconfigurable metasurfaces has been furthered by introducing active devices such as pin diodes [8–10], varactor diodes [11–13], and MEMS switches [14,15] into metaparticles. The dynamic modulation of these active components, via external control signals, enables the reconfigurability of the metasurfaces. However, integrating components with dynamic control in a conformal platform is more challenging.

Microwave holograms are created based on the theory of optical holography [16]. By recording the phase and amplitude information of the incident electromagnetic wave and precisely designing the surface impedance, the desired interference pattern can be generated in the far field. It makes holographic metasurfaces (HMs) widely applicable in fields such as wireless communications systems [17–19]. If holography is combined with reconfigurable technology, multiple functions can be realized without physical replacement or modification, thus enhancing the versatility and adaptability of the system. Furthermore, HMs are easy to achieve conformal design [20], which allows them to be integrated into complex structures more easily.

Most of the implemented tunable metasurfaces focus on the reconfigurability of individual functions, such as beam steering [21–23], polarization control [24–26], and low scattering [27–29]. Recent research has been devoted to the design of multifunctional integrated tunable metasurfaces [30–34], which are used to satisfy complex electromagnetic environments. They not only improve the overall performance of the system but also reduce the complexity and cost, bringing new opportunities for the development of radar systems. In this paper, a multifunctional dynamic modulation mechanism of radiation and scattering based on reconfigurable HM is proposed for conformal applications. The conformal surface impedance distribution of HM is derived. A compact conformal prototype containing 440 reconfigurable HM unit cells and a monopole is designed and fabricated to verify the mechanism. Switching between different modes is achieved by integrating only one varactor diode on each HM unit cell, as shown in Fig. 1.

- 1) Function I: Radiation beam forming. In the radiation mode, dynamic beam forming is achieved with beam coverage ranging from -50° to 50° , ensuring the flexibility and directivity of the radiation beam.
- 2) Function II: Reflected beam steering. In the scattering mode, the reflected beam steering modulation under oblique incident wave within $\pm 60^\circ$ is achieved, enhancing the focusing of the reflected beam.
- 3) Function III: Reflected beam splitting. Multi-beam splitting within $\pm 60^\circ$ is realized under normal incident wave, which enhances the directionality and controllability of the beam.
- 4) Function IV: Diffuse reflection. The radar cross section (RCS) is effectively reduced through scattering suppression.

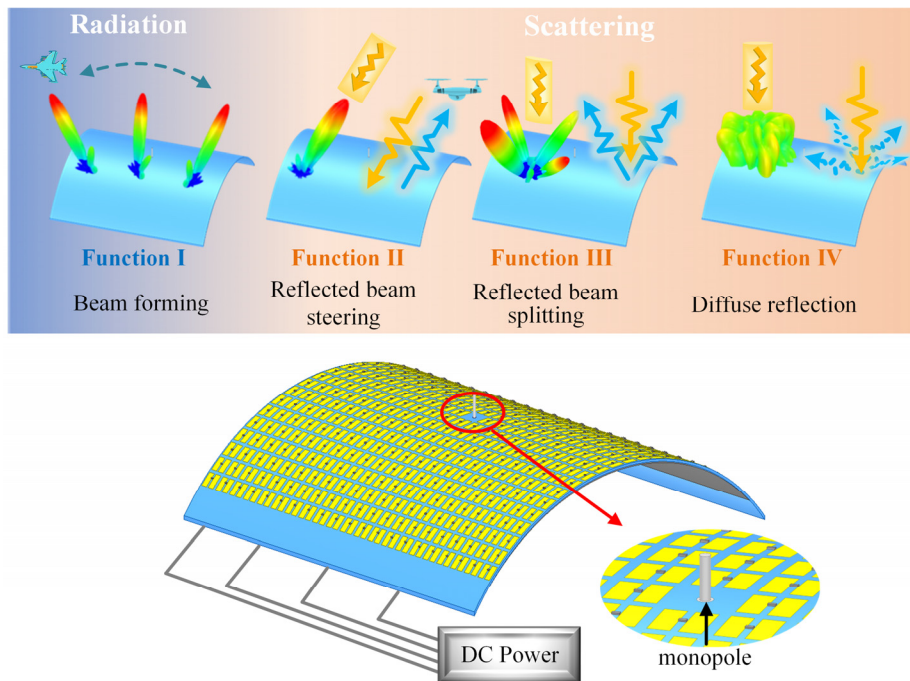


Fig. 1. Schematic of the conformal reconfigurable HM and its functions.

The paper is organized as follows. Section 2 elaborates in detail on the electromagnetic wave modulation mechanism of the conformal reconfigurable HM. Section 3 serves as a proof of concept, four functions of the conformal reconfigurable HM are simulated exemplarily. a reconfigurable HM prototype is fabricated and four functions are demonstrated as described in Section 4. The designed conformal reconfigurable HM has excellent angular stability and adaptability to cylindrical platform, which has important practical value for the communication system and stealth of conformal platform.

2. Design and mechanism

Figure 2 illustrates the structure of the HM unit cell, which contains three metal layers separated by two dielectric substrates. The top metal layer includes two identical rectangular patches symmetrically placed about the x -axis. A varactor diode is embedded in the gap between the two patches to achieve reconfigurability of HM. The middle metal layer is covered by a copper plate used as ground. The metal vias pass through the hole in the ground and connect to the DC control lines at the bottom layer. By controlling the varactor diode from the back side of the surface in this way, the bias lines do not interfere with the microwave field on the front side. Both substrates are Taconic RF-60TC with a relative permittivity of 6.15 and a loss tangent of 0.0028. Based on the simulation software optimization, key geometric dimensions are: $a = 5$ mm (approximately $0.167\lambda@10$ GHz), $g = 1.4$ mm, $h_1 = 1.27$ mm, and $h_2 = 0.128$ mm. The diameters of the vias are $d_1 = 0.7$ mm and $d_2 = 0.6$ mm. Based on the actual voltage-capacitance characteristics of the varactor diode, corresponding capacitance values are set for the varactor diode model in the simulation. Here the varactor diode is SMV1232-040LF [35], and the capacitance can be tuned from 4.15 to 0.72 pF under reverse bias from 0 to 20 V.

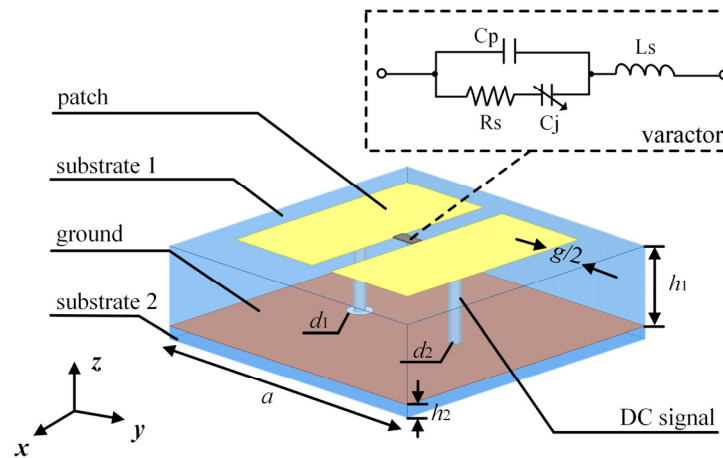


Fig. 2. Geometry of the reconfigurable HM unit cell.

The HM is the presentation of the interference pattern of the reference wave and the desired wave. The reference wave is ψ_{ref} . The desired wave is ψ_{obj} . The surface impedance of HM is expressed as [16]

$$Z = j[X + M\text{Re}(\psi_{obj}\psi_{ref}^*)] \quad (1)$$

where X is the average impedance of the HM and M is the modulation depth.

The HM unit cell is simulated using HFSS software and its performance is verified and optimized. The plane wave is incident on the upper surface of the HM, using periodic boundary condition and Floquet port. The simulated dispersion curves of different capacitance unit cells of

the reconfigurable HM and the fitting curve of calculated surface impedance versus capacitance are shown in Fig. 3(a). The fitting results indicate that as the capacitance value increases, the surface impedance of the HM unit cells increases. Figure 3(b) presents the simulated reflection amplitude and phase response of different capacitance cells under plane wave incidence at angles of -60° , -20° , 0° , 20° , and 60° . It can be seen that the reflection amplitudes and phase gradients of different capacitive cells remain largely consistent at 10 GHz. Furthermore, the reflection amplitudes and phase responses of the cells exhibit stable angular insensitivity at different incident angles.

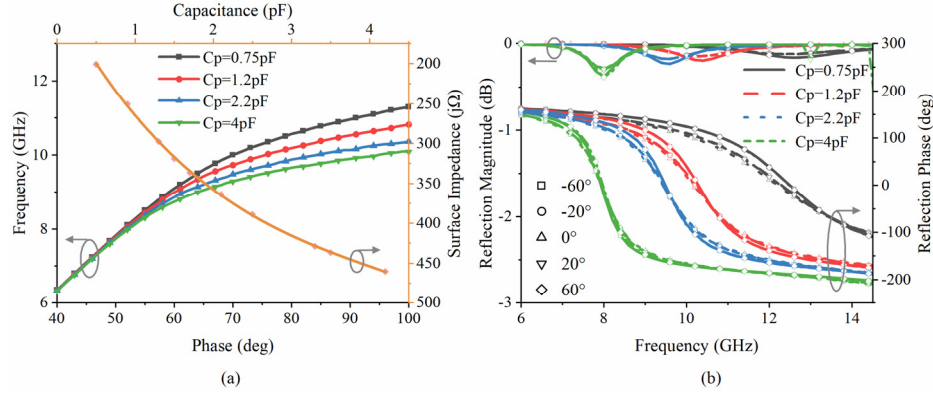


Fig. 3. Reconfigurable HM unit cell characteristics. (a) Simulated dispersion curves of different capacitance unit cells and the fitting curve of calculated surface impedance versus capacitance value. (b) Simulated reflection amplitudes and phase responses of different capacitance unit cells for different incident angles.

The functional relationship between the surface impedance and capacitance value of the reconfigurable HM obtained by fitting is given by

$$Z = j(1.546^{-7}c^3 - 1.12^{-4}c^2 + 0.035c - 3.6). \quad (2)$$

The schematic of the reference wave and desired wave in different functional modes of the conformal reconfigurable HM is shown in Fig. 4, where r_0 is the radius of the cylindrical substrate. In the radiation mode, the monopole located at the center of the HM serves as the excitation source, and the surface wave it excites is considered the reference wave. The reference wave is further excited to generate radiation wave, which is regarded as the desired wave. The reference wave and desired wave of Function I are respectively

$$\psi_{ref1} = \exp(-jk_0nr) \quad (3)$$

$$\psi_{obj1} = \exp(-j\vec{k}_0 \cdot \vec{r}) \quad (4)$$

where k_0 is the wavenumber in free space, n is the average surface refractive index of the HM, r is the distance from the excitation source to the point on the surface, \vec{k}_0 is the radiation wave vector, and \vec{r} is the coordinate of the point on the surface.

Combining (1), the surface impedance modulation for the conformal HM in radiation mode of Function I can be derived as

$$Z_1 = j \left[X + M \cos \begin{pmatrix} k_0 n \sqrt{(r_0 \sin^{-1}(x/r_0))^2 + y^2} \\ -k_0 x \cos \varphi_2 \sin \theta_2 - k_0 y \sin \varphi_2 \sin \theta_2 \\ -k_0 (r_0 \cos(\sin^{-1}(x/r_0)) - r_0) \cos \theta_2 \end{pmatrix} \right] \quad (5)$$

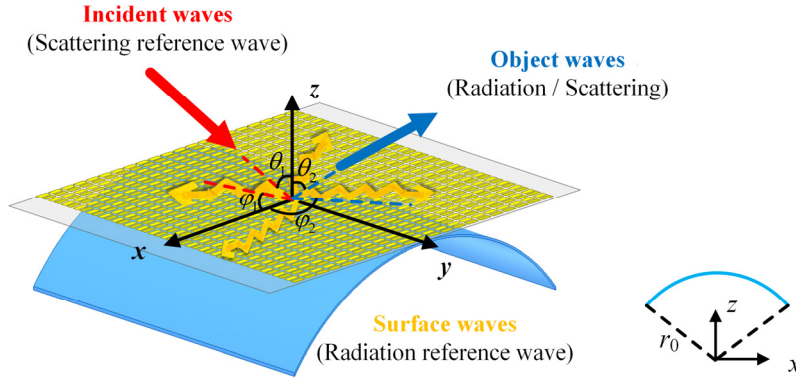


Fig. 4. Schematic of multifunctional radiation and scattering modulation for conformal reconfigurable HM.

where r_0 is the radius of the cylindrical substrate, θ_2 is the elevation angle of the desired wave, and φ_2 is the azimuth angle of the desired wave.

In the scattering beam steering modulation mode, the incident plane wave is set as the reference wave and the scattering field generated by the plane wave excitation is taken as the desired field. The reference wave and desired wave of Function II are respectively

$$\psi_{ref2} = \exp(-j\vec{k}_r \cdot \vec{r}) \quad (6)$$

$$\psi_{obj2} = \exp(-j\vec{k}_s \cdot \vec{r}) \quad (7)$$

where \vec{k}_r is the incident wave vector and \vec{k}_s is the desired wave vector.

The surface impedance modulation formula for the conformal HM of Function II is:

$$Z_{II} = j \left[X + M \cos \begin{pmatrix} k_0 x \sin \theta_1 \cos \varphi_1 + k_0 y \sin \theta_1 \sin \varphi_1 \\ +k_0(r_0 \cos(\sin^{-1}(x/r_0)) - r_0) \cos \theta_1 \\ -k_0 x \sin \theta_2 \cos \varphi_2 - k_0 y \sin \theta_2 \sin \varphi_2 \\ -k_0(r_0 \cos(\sin^{-1}(x/r_0)) - r_0) \cos \theta_2 \end{pmatrix} \right] \quad (8)$$

where θ_1 is the elevation angle of the reference wave, φ_1 is the azimuth angle of the reference wave, and θ_2 and φ_2 are the same as those in (5).

The reference wave and desired wave of Function III are respectively

$$\psi_{ref3} = \exp(-jk_0(r_0 \cos(\sin^{-1}(x/r_0)) - r_0)) \quad (9)$$

$$\psi_{obj3} = \psi_{obj2}. \quad (10)$$

The reference wave of Function IV is the incident plane wave, and the desired wave is the surface wave to reduce RCS. The reference wave and desired wave for diffuse reflection mode of Function IV are respectively

$$\psi_{ref4} = \psi_{ref2} \quad (11)$$

$$\psi_{obj4} = \psi_{ref1}. \quad (12)$$

Based on the above formula, the electromagnetic properties of the HM unit cells at different position can be accurately analyzed and controlled in multiple functional states. The precise control of the radiation and scattering waves can be achieved in the far-field by field superposition.

3. Multifunctional radiation and scattering modulation

A reconfigurable HM composed of 440 cells is constructed and analyzed by HFSS full wave simulations. Four functions realized by the designed reconfigurable HM are verified.

3.1. Radiation beam forming

The reconfigurable HM is conformally applied to a cylindrical substrate with a radius of $r_0 = 160$ mm. The simulated reflection coefficients of a single monopole and different radiation scanning states of Function I are given in Fig. 5(a). The reflection coefficients of all states are below -10 dB in the frequency range of 9.3~11.8 GHz, demonstrating good impedance matching characteristics. As shown in Fig. 5(b), the simulated 2-D radiation pattern of the conformal reconfigurable HM in the yo_z plane at 10 GHz is depicted. Multiple beams are formed between $\pm 50^\circ$, with a scanning loss of 2.6 dB between the gain of the $\pm 50^\circ$ beams and the maximum gain of $\pm 20^\circ$ beam, maintaining low loss characteristics under wide-angle scanning.

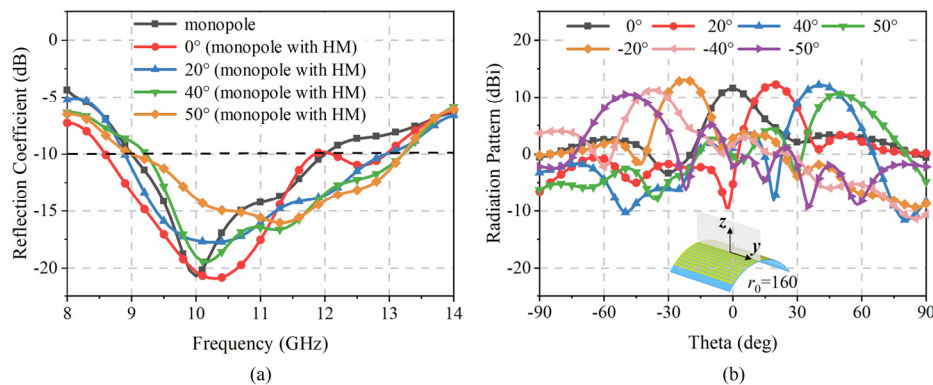


Fig. 5. Demonstration of Function I. (a) Simulated reflection coefficients with different scanning states. (b) Simulated 2-D radiation patterns for beam forming at typical angles in the yo_z plane at 10 GHz. with conformal reconfigurable HM excited by monopole.

Figure 6 shows the 3-D radiation pattern and the distribution of the varactor diode for different radiation scanning states. From the capacitance value distribution, it can be observed that as the radiation angle increases, the period of the capacitance distribution along the radiation direction becomes larger, and the trend is shifted towards the radiation direction. It is demonstrated that the reconfigurable HM achieves radiation dynamic beamforming by controlling the capacitance of the varactor diode without changing the base unit structure.

3.2. Reflected beam steering

In order to investigate the ability of the reconfigurable HM to modulate the scattering characteristics, the reconfigurable HM is conformal on a cylindrical substrate with a radius of 160 mm, and the excitation source antenna is connected to a 50Ω matched load. The incident plane wave serves as the reference wave.

Figure 7(a) presents the simulated scattering patterns at 10 GHz in the yo_z plane under different angles of incident wave, where the reflection direction is consistent with the incident direction. The designed conformal reconfigurable HM in Function II demonstrates significant insensitivity to oblique incidence, achieving stable and continuous scattering beam steering within the range of $\pm 60^\circ$ incident angles. Figure 7(b) displays the scattering patterns of the conformal reconfigurable HMs with different curvatures under -60° and 60° oblique incidence. The results indicate that all

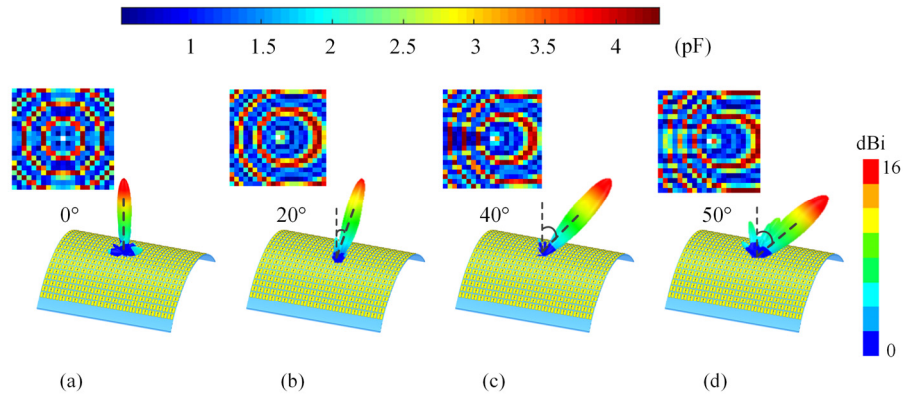


Fig. 6. Simulated 3-D radiation patterns and the capacitance distribution for different states of Function I. The radiation beam deflection angle θ_2 is (a) 0° (b) 20° (c) 40° (d) 50° .

reconfigurable HM can produce stable deflected beams, validating their stability and reliability in directing scattering beams under different conformal curvature conditions.

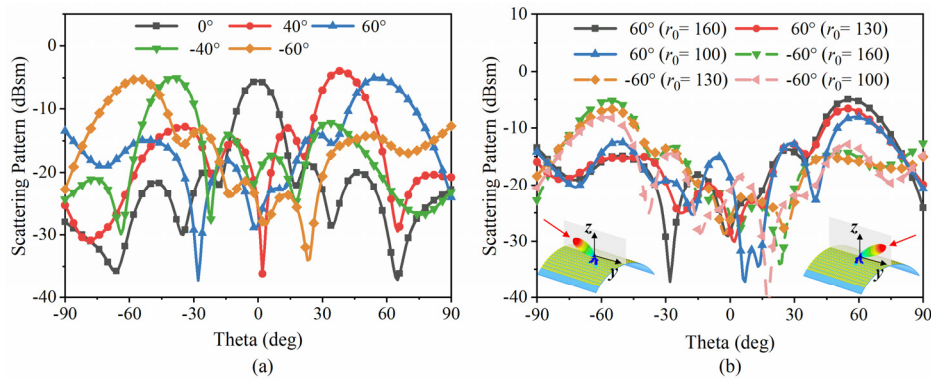


Fig. 7. Demonstration of Function II. Simulated scattering patterns at 10 GHz in the $yo z$ plane under oblique incidence. (a) The incidence angles are 0° , 40° , 60° , -40° , and -60° . The radius of cylindrical substrate is 160 mm. (b) The incidence angles are 60° and -60° . The radius of cylindrical substrate is 160 mm, 130 mm, and 100 mm, respectively.

3.3. Reflected beam splitting

The scattering of periodic metasurfaces under normal incident plane wave can be explained by grating theory [36]. The normal incident plane wave is scattered into symmetric angular directions ($m = \pm 1$ diffraction mode) besides the specular reflection ($m = 0$ diffraction mode). By applying the generalized Snell's law of reflection, the direction of the scattering beam is determined as:

$$\theta_n = \sin^{-1} \left(\frac{\beta_0}{k_0} + \frac{2m\pi}{k_0 p} \right) \quad (13)$$

where $m = 0, \pm 1, \pm 2, \dots$

According to (13), the designed reconfigurable HM naturally generates dual-beam splitting at symmetric angles under normal incident plane wave. Figure 8(a) shows the scattering patterns of the conformal reconfigurable HM at 10 GHz, where dual beams are deflected at angles of

$\pm 45^\circ$ in the planes of $\varphi = 45^\circ$ and $\varphi = 135^\circ$ under normal incidence. Figure 8(b) demonstrates the scattering patterns of conformal reconfigurable HMs with different curvatures, achieving $\pm 60^\circ$ dual-beam splitting in the $yo z$ plane under normal incidence. The results indicate that the reconfigurable HM maintains a stable control over the direction of the scattering dual beams.

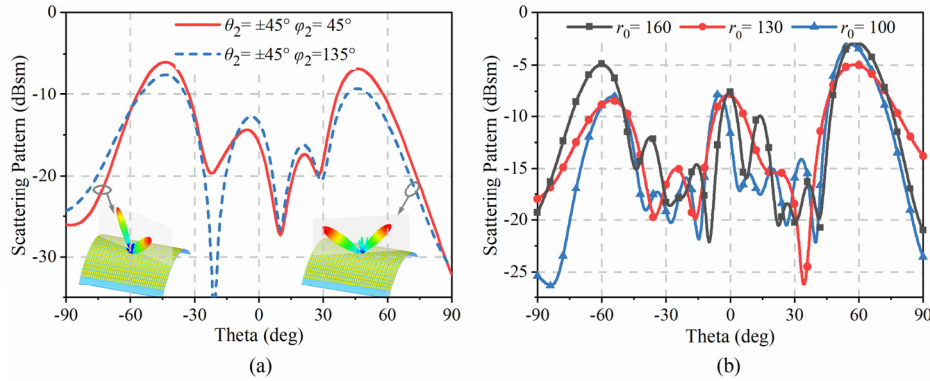


Fig. 8. Demonstration of Function III. Simulated scattering pattern of dual-beam splitting at 10 GHz under normal incident plane wave. (a) $\pm 45^\circ$ beams in the $\varphi = 45^\circ$ and $\varphi = 135^\circ$ plane, respectively. The radius of cylindrical substrate is 160 mm. (b) $\pm 60^\circ$ beams in the $yo z$ plane. The radius of cylindrical substrate is 160 mm, 130 mm, and 100 mm, respectively.

Furthermore, Fig. 9 shows the quad-beam splitting capability of conformal reconfigurable HM under normal incidence. It is capable of generating four beams simultaneously within the same plane, as depicted in Fig. 9(a), and dual beams in two orthogonal planes, as shown in Fig. 9(b) and (c). This demonstrates the ability of the designed reconfigurable HM in Function III to achieve precise multi-beam splitting within $\pm 60^\circ$.

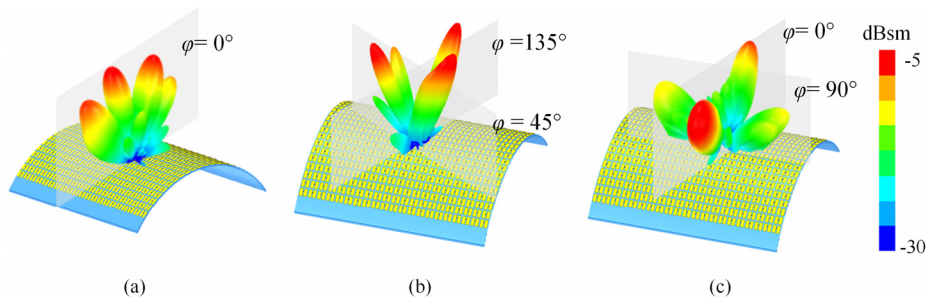


Fig. 9. Demonstration of Function III. Simulated scattering pattern of quad-beam splitting under normal incident plane wave. (a) $\pm 20^\circ$ and $\pm 40^\circ$ beams in the $\varphi = 0^\circ$ plane, (b) $\pm 20^\circ$ beams in the $\varphi = 45^\circ$ plane and $\varphi = 135^\circ$ plane, and (c) $\pm 60^\circ$ beams in the $\varphi = 0^\circ$ and $\varphi = 90^\circ$ plane.

3.4. Diffuse reflection

In addition to directional beam modulation for information transmission, the designed conformal reconfigurable HM also possesses the capability to achieve diffuse reflection. Figure 10(a) shows the monostatic RCS of monopole with conformal reconfigurable HM of radius 160 mm and a monopole with the same size under normal incident wave. It can be observed from 3-D scattering pattern at 10 GHz that monostatic RCS is significantly reduced in the normal direction and there

is no obvious beam in other directions, which realizes diffuse reflection and effective suppression of scattering.

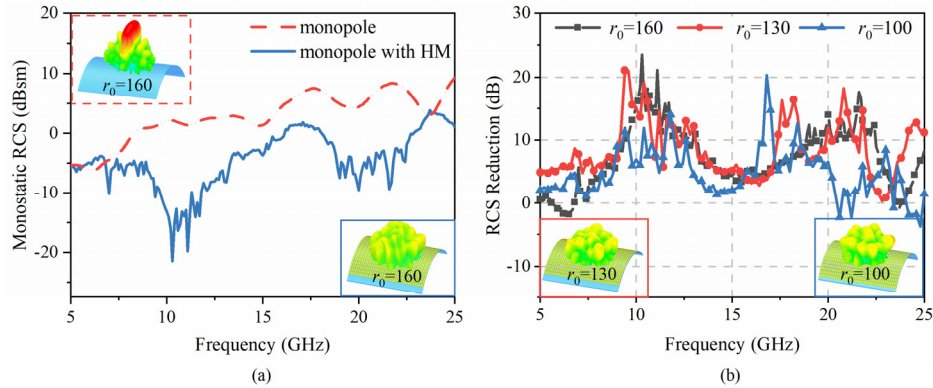


Fig. 10. Demonstration of function IV. (a) Simulated monostatic RCS of monopole with reconfigurable HM of 160 mm radius and monopole of the same size. (b) Simulated monostatic RCS reduction of reconfigurable HM. The radius of cylindrical substrate is 160 mm, 130 mm, and 100 mm, respectively. and 3-D scattering patterns at 10 GHz.

Figure 10(b) presents the RCS reduction with different radii and the 3-D scattering patterns at 10 GHz for radii of 130 mm and 100 mm. In particular, the RCS reduction is obtained for the conformal HM with a radius of 160 mm over a wide band ranging from 6.8 GHz to 23.6 GHz. At 10.3 GHz, the RCS reduction reaches 23.5 dB. It is evident that the conformal reconfigurable HM can maintain stable diffuse reflection performance and broadband RCS reduction capability.

4. Prototype fabrication and measured results

The conformal reconfigurable HM prototype is shown in Fig. 11(a), with a total area of 185×185 mm² ($6.17\lambda \times 6.17\lambda$ mm² @ 10 GHz), a total thickness of 1.6 mm, and a conformal cylindrical radius of 160 mm. Due to the continuous tunable capacitance characteristic of varactor diodes, diverse electromagnetic properties can theoretically be achieved by selecting the appropriate varactor diode. In the measurement scheme, varactor diodes with the same bias voltage are grouped and made to share the same voltage source. This design strategy simplifies the design of the bias circuit and maintains precise control over electromagnetic characteristics.

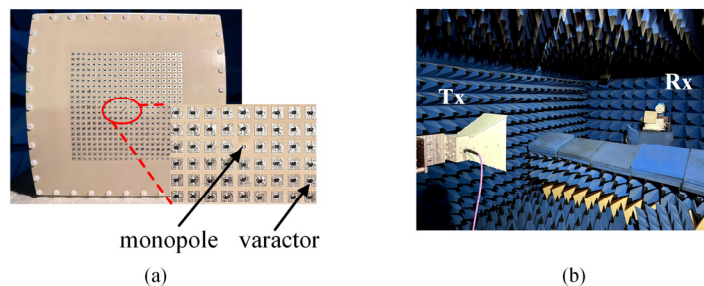


Fig. 11. Designed conformal reconfigurable HM experimental validation. (a) Photograph of fabricated prototype. (b) Measurement setup in microwave anechoic chamber of radiation mode.

Figure 11(b) illustrates the measurement setup in microwave anechoic chamber of radiation mode, where a standard gain horn antenna is used as the transmitting antenna. Figure 12 presents the experimental validation of Function I. The measured reflection coefficients with various radiation states are all below -10 dB at 10 GHz, indicating excellent impedance matching. The measured radiation beams can be accurately steered to the preset angles, which confirms the stable radiation beam modulation capability of the designed conformal reconfigurable HM in Function I. Compared to the simulated results, the main lobe gain of the measured radiation pattern is lower, which may be due to uncertainties in the circuit connections.

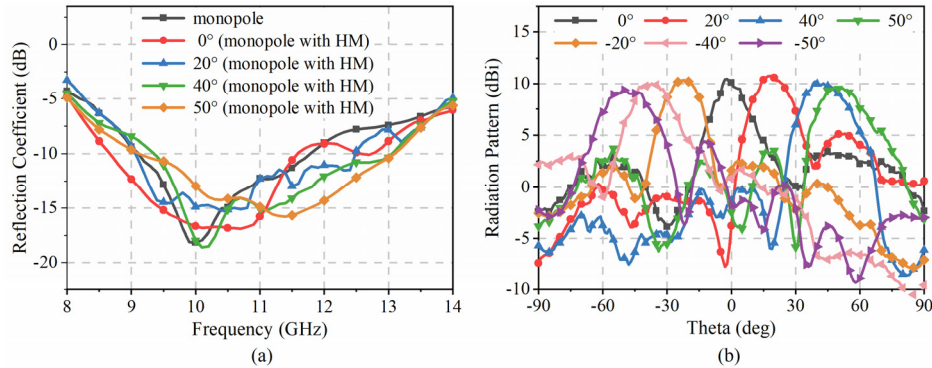


Fig. 12. Experimental verification of Function I. (a) Measured reflection coefficients with different scanning states. (b) Measured 2-D radiation patterns at 10 GHz in the yoz plane for beam forming from -50° to 50° .

For the scattering mode measurements, the prototype is located in the far field of the horn antenna, with a 50Ω matched load connected to the feeding port of the monopole. The substrate is wrapped in absorbing material to suppress undesired reflections, as shown in Fig. 13(a) and (b). Figure 14(a) and (b) demonstrate that the reflected beam is redirected to 40° and 50° , respectively, with the reflection direction consistent with the incidence direction. Figure 14(c) to (e) exhibit the achievement of dual-beam splitting within the $\pm 60^\circ$ range under normal incidence, thereby validating the insensitivity of the designed conformal reconfigurable HM to the angle of incidence. By designing the voltage configuration applied to the varactor diodes, more beam deflection angles can be obtained. Factors contributing to the differences in angle deflection is primarily due to the inhomogeneity of the sample, which is caused by imperfections in the fabrication procedure. Additionally, since the simulation is conducted under ideal conditions, there are interferences in the test environment that cannot be fully modeled in the simulation.

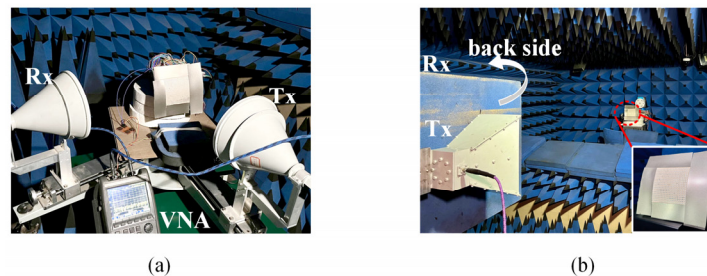


Fig. 13. Designed conformal reconfigurable HM experimental validation. Measurement setup in microwave anechoic chamber of (a) Function II, Function III, and (b) Function IV.

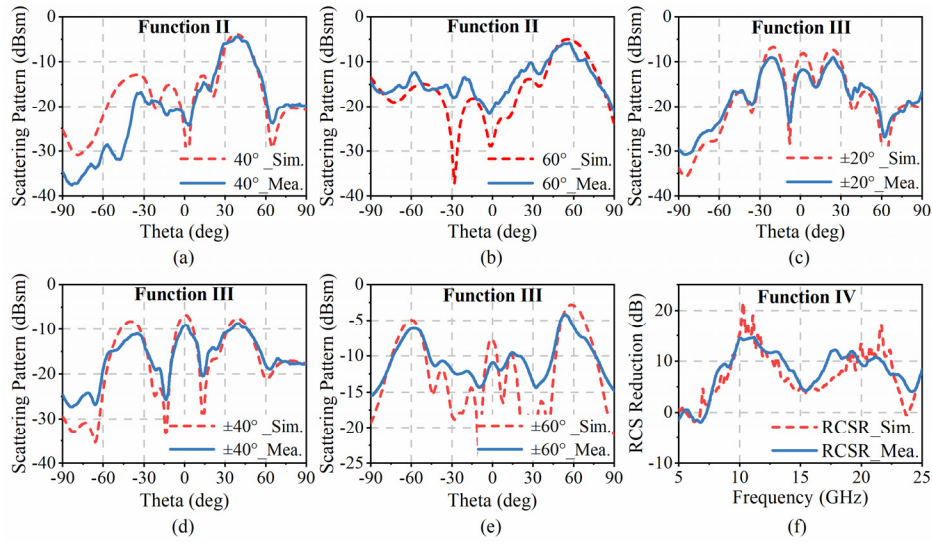


Fig. 14. Experimental demonstration of the scattering function. (a)-(b) Function II: beam steering. (a) Reflected waves deflected to 40° under oblique 40° incident plane wave. (b) Reflected waves deflected to 60° under oblique 60° incident plane wave. (c)-(e) Function III: beam splitting. Dual beams of (c) $\pm 20^\circ$ (d) $\pm 40^\circ$ and (e) $\pm 60^\circ$ under normal incident plane wave. f) Function IV: diffuse reflection. RCSR of conformal reconfigurable HM with a curvature radius of 160 mm.

The broadband RCS reduction capability of Function IV is shown in Fig. 14(f), where RCS reduction is achieved from 7.2 to 25 GHz, with the maximum RCS reduction of 16.45 dB at 10.8 GHz. Overall, the measurement and simulation results for the four functions are in good agreement, confirming the feasibility of integrating dynamic control of radiation and scattering into a conformal reconfigurable HM as proposed.

In terms of achievable functionalities and implementation complexity, the designed conformal reconfigurable HM has been compared with other active metasurface technologies reported in the open literature in Table 1. In [30] and [33], only modulated scattering modes are achieved using pin diodes and varactor diodes respectively. In [31], two types of varactor diodes are used to realize single-beam and multi-beam radiation. Pin and varactor diodes are utilized to achieve functions of single-beam deflection and multi-beam splitting in [32]. A bi-functional

Table 1. Performance Comparison of Designed Reconfigurable HM with Previous Works

| Ref. | Control component (number) | Frequency band (GHz) | | Number of demonstration functions | | Angular range | Conformal |
|------------------|----------------------------|----------------------|---------------|-----------------------------------|------------|----------------------------------|------------|
| | | Radiation | Scattering | Radiation | Scattering | | |
| [30] | Pin-diode (1) | / | 9~12 | 0 | 3 | 40° | No |
| [31] | Varactor (2) | 5 | / | 2 | 0 | $\pm 36^\circ$ | No |
| [32] | Pin-diode & Varactor (2) | / | 6.3~13 | 0 | 3 | 43° | No |
| [33] | Varactor (1) | / | 7~13 | 0 | 2 | 60° | Yes |
| [34] | Varactor (4) | 1.65~2.25 | 1.24~2.23 | 1 | 1 | / | No |
| This work | Varactor (1) | 9.3~11.8 | 7.2~25 | 1 | 3 | $\pm 60^\circ$ | Yes |

design for radiation and scattering is realized in [34] using four varactor diodes. In contrast, the conformal multifunctional design proposed in this work, by integrating only one varactor diode, achieves modulation of radiation and scattering for conformal applications, while also maintaining insensitivity to changes in the angle of incidence and stability in controlling deflection angles.

5. Conclusion

A mechanism that integrates multifunctional dynamic radiation and scattering modulation capabilities into conformal HM is presented in this paper. The dynamic control of electromagnetic waves in predetermined directions is achieved by embedding a varactor diode within the HM cells. Four functions are demonstrated using the designed conformal reconfigurable HM, including, but is not limited to, radiation beam forming, reflection beam steering for arbitrary angles of oblique incidence, multi-beam splitting under normal incidence, and diffuse reflection. The designed conformal reconfigurable HM exhibits adaptability to cylindrical platform, insensitivity to incidence angle variations, and stability in modulated beam deflection angles. These characteristics provide significant advantages and broad application potential in the fields of radar detection and communication on conformal platform.

Funding. National Natural Science Foundation of China (62201417, 62171335).

Disclosures. The authors declare no conflicts of interest.

Data availability. Data underlying the results presented in this paper are not publicly available at this time but may be obtained from the authors upon reasonable request.

References

1. Z. Huang, Y. Zheng, J. Li, *et al.*, "High-resolution metalens imaging polarimetry," *Nano Lett.* **23**(23), 10991–10997 (2023).
2. D. Wang, L. Yang, B. Cai, *et al.*, "Temperature tunable broadband filter based on hybridized vanadium dioxide (VO₂) metasurface," *Journal of Physics D: Applied Physics* **58**(3), 035106 (2025).
3. Y. Sun, B. Cai, L. Yang, *et al.*, "High-gain dual-polarization microstrip antenna based on transmission focusing metasurface," *Materials* **17**(15), 3730 (2024).
4. M. Deng, M. Cotrufo, J. Wang, *et al.*, "Broadband angular spectrum differentiation using dielectric metasurfaces," *Nat. Commun.* **15**(1), 2237 (2024).
5. M. Deng, S. Kanwal, Z. Wang, *et al.*, "Dielectric metasurfaces for broadband phase-contrast relief-like imaging," *Nano Lett.* **24**(46), 14641–14647 (2024).
6. N. Han, L. Huang, and Y. Wang, "Illusion and cloaking using dielectric conformal metasurfaces," *Opt. Express* **26**(24), 31625–31635 (2018).
7. X. Xu, B. Peng, D. Li, *et al.*, "Flexible visible–infrared metamaterials and their applications in highly sensitive chemical and biological sensing," *Nano Lett.* **11**(8), 3232–3238 (2011).
8. X. Wan, Z. A. Huang, J. W. Wang, *et al.*, "Information metasurface for electromagnetic sensing and wireless communications," *Adv. Mater. Technol.* **9**(2), 1–9 (2024).
9. X. Wan, C. K. Xiao, H. Huang, *et al.*, "User tracking and wireless digital transmission through a programmable metasurface," *Adv. Mater. Technol.* **6**(7), 2001254 (2021).
10. B. Zeng, C. Li, H. Cheng, *et al.*, "Anisotropic programmable metasurface beam splitter based on diode real-time control," *Opt. Lasers Eng.* **169**, 107723 (2023).
11. W. Tang, X. Li, J. Y. Dai, *et al.*, "Wireless communications with programmable metasurface: Transceiver design and experimental results," *China Commun.* **16**(5), 46–61 (2019).
12. B. O. Zhu, K. Chen, N. Jia, *et al.*, "Dynamic control of electromagnetic wave propagation with the equivalent principle inspired tunable metasurface," *Sci. Rep.* **4**(1), 4971 (2014).
13. C. X. Huang, J. Zhang, Q. Cheng, *et al.*, "Polarization modulation for wireless communications based on metasurfaces," *Adv. Funct. Mater.* **31**(36), 2103379 (2021).
14. P. Pitchappa, C. P. Ho, L. Cong, *et al.*, "Reconfigurable digital metamaterial for dynamic switching of terahertz anisotropy," *IEEE Trans. Terahertz Sci. Technol.* **5**(6), 803–811 (2015).
15. C. Guclu, J. Perruisseau-Carrier, and O. Civi, "Proof of concept of a dual-band circularly-polarized RF MEMS beam-switching reflectarray," *IEEE Trans. Antennas Propag.* **60**(11), 5451–5455 (2012).
16. B. H. Fong, J. S. Colburn, J. J. Ottusch, *et al.*, "Scalar and tensor holographic artificial impedance surfaces," *IEEE Trans. Antennas Propag.* **58**(10), 3212–3221 (2010).
17. S. Ramalingam, C. A. Balanis, C. R. Birtcher, *et al.*, "Polarization diverse holographic metasurfaces," *IEEE Antennas Wireless Propag. Lett.* **18**(2), 264–268 (2019).

18. S. Pandi, C. A. Balanis, and C. R. Birtcher, "Design of scalar impedance holographic metasurfaces for antenna beam formation with desired polarization," *IEEE Trans. Antennas Propag.* **63**(7), 3016–3024 (2015).
19. V. R. Gowda, M. F. Imani, T. Sleasman, *et al.*, "Focusing microwaves in the Fresnel zone with a cavity-backed holographic metasurface," *IEEE Access* **6**, 12815–12824 (2018).
20. D. Sievenpiper, J. Colburn, B. Fong, *et al.*, "Holographic artificial impedance surfaces for conformal antennas," *Proc. IEEE Antennas Propag. Soc. Int. Symp.* **1**, 256–259 (2005).
21. Y.B. Li, X. Wan, B.G. Cai, *et al.*, "Frequency-controls of electromagnetic multi-beam scanning by metasurfaces," *Sci. Rep.* **4**(1), 6921 (2014).
22. T. Z. Fadhil, N. A. Murad, M. K. A. Rahim, *et al.*, "A beam-split metasurface antenna for 5 G applications," *IEEE Access* **10**, 1162–1174 (2021).
23. J. Wang and R. Yang, "Generating high-purity directive circularly polarized beams from conformal anisotropic holographic metasurfaces," *IEEE Trans. Antennas Propag.* **70**(11), 10718–10723 (2022).
24. Z. Xu, C. Ni, Y. Cheng, *et al.*, "Photo-excited metasurface for tunable terahertz reflective circular polarization conversion and anomalous beam deflection at two frequencies independently," *Nanomaterials* **13**(12), 1846 (2023).
25. Y. Cheng, C. Rong, J. Li, *et al.*, "Dual-band terahertz reflective-mode metasurface for the wavefront manipulation of independent linear and circular polarization waves," *JOSA B* **41**(2), 341–350 (2024).
26. Y. He, B. Cai, L. Wu, *et al.*, "Tunable VO₂ metasurface for reflective terahertz linear and circular polarization wavefront manipulation at two frequencies independently," *Phys. B* **681**, 415848 (2024).
27. M. Heidari, S. H. Sedighy, and M. K. Amirhosseini, "RCS reduction using grounded multi-height multi-dielectrics metasurfaces," *Sci. Rep.* **13**(1), 3069 (2023).
28. Y. Wang, J. Su, Z. Li, *et al.*, "A prismatic conformal metasurface for radar cross-sectional reduction," *IEEE Antennas Wireless Propag. Lett.* **19**(4), 631–635 (2020).
29. W. Chen, C. A. Balanis, C. R. Birtcher, *et al.*, "Cylindrically curved checkerboard surfaces for radar cross-section reduction," *IEEE Antennas Wireless Propag. Lett.* **17**(2), 343–346 (2018).
30. H. Yang, X. Cao, F. Yang, *et al.*, "A programmable metasurface with dynamic polarization, scattering and focusing control," *Sci. Rep.* **6**(1), 1–11 (2016).
31. Y. Fan, J. Chen, and C. Mou, "Pattern-reconfigurable integrated array antenna based on a coding metasurface," *Opt. Express* **32**(6), 8816–8827 (2024).
32. C. Huang, C. Zhang, J. Yang, *et al.*, "Reconfigurable metasurface for multifunctional control of electromagnetic waves," *Adv. Opt. Mater.* **5**(22), 1700485 (2017).
33. Y. Shang, S. Wang, C. Liao, *et al.*, "Dynamic augmentation of scattering cross-section by a conducting polycylinder coated with varactor-loaded metasurface," *IET Microw. Antenna* **15**(8), 835–842 (2021).
34. C. Zhang, J. Gao, X. Cao, *et al.*, "Multi-functional tunable metasurface for radiation and scattering manipulation," *IET MICROW ANTENNA* **13**(15), 2649–2653 (2019).
35. Skyworks Solutions. *SMV1232-040LF*. Accessed: Jun. 2024. [Online]. Available: https://www.skyworksinc.com/-/media/SkyWorks/Documents/Products/101-200/SMV123x_Series_200058AA.pdf.
36. A. Wirgin, "Scattering from sinusoidal gratings: an evaluation of the Kirchhoff approximation," *J. Opt. Soc. Am.* **73**(8), 1028–1041 (1983).